


Article

Structural and Mechanical Characteristics of $\text{Cu}_{50}\text{Zr}_{43}\text{Al}_7$ Bulk Metallic Glass Fabricated by Selective Laser Melting

Xiaoyang Lu ^{1,2} , Mussokulov Nursulton ¹, Yulei Du ^{1,*} and Wenhe Liao ^{1,*}

¹ School of Mechanical Engineering, Nanjing University of Science and Technology, Nanjing 210094, China; njust_luxiaoyang@163.com (X.L.); ac_milan_barsa@mail.ru (M.N.)

² Luoyang Ship Material Research Institute, Luoyang 471023, China

* Correspondence: yldu_njust@njust.edu.cn (Y.D.); cnwho@njust.edu.cn (W.L.)

Received: 9 December 2018; Accepted: 31 January 2019; Published: 6 March 2019



Abstract: In this work, the structural and mechanical characteristics of $\text{Cu}_{50}\text{Zr}_{43}\text{Al}_7$ bulk metallic glass (BMG) fabricated by selective laser melting (SLM) are studied and the impacts from the SLM process are clarified. $\text{Cu}_{50}\text{Zr}_{43}\text{Al}_7$ alloy specimens were manufactured by the SLM method from corresponding gas-atomized amorphous powders. The as-built specimens were examined in terms of phase structure, morphologies, thermal properties and mechanical behavior. The x-ray diffraction and differential scanning calorimetry results showed that structural relaxation and partial crystallization co-exist in the as-fabricated $\text{Cu}_{50}\text{Zr}_{43}\text{Al}_7$ glassy samples. The nano- and micro- hardness and the elastic modulus of the SLM-fabricated $\text{Cu}_{50}\text{Zr}_{43}\text{Al}_7$ BMG were higher than CuZrAl ternary BMGs with similar compositions prepared by conventional mold casting, which can be attributed to the structural relaxation in the former sample. However, the macro compressive strength of the SLM-fabricated $\text{Cu}_{50}\text{Zr}_{43}\text{Al}_7$ BMG was only 1044 MPa mainly due to its porosity. This work suggests that the SLM process induced changes in structural and mechanical properties are significant and cannot be neglected in the fabrication of BMGs.

Keywords: bulk metallic glasses; selective laser melting; $\text{Cu}_{50}\text{Zr}_{43}\text{Al}_7$; mechanical properties

1. Introduction

Bulk metallic glasses (BMGs) are promising structural materials because of their unique mechanical, physical and chemical properties [1–3]. However, due to their limited ability to form glass, it is difficult to fabricate BMGs with large cross sections or complex shapes by traditional mold casting methods. To overcome such size and shape restrictions, powder metallurgy methods, such as hot-pressing sintering and spark plasma sintering techniques, have been adopted to prepare BMGs [4,5]. However, the consolidation of amorphous powders into bulk samples by these methods requires high pressure and molds. So, the manufacturing of large BMGs with complex shapes remains a problem. Selective laser melting (SLM), a laser additive manufacturing technique, can obtain a cooling rate as high as 10^3 – 10^4 K/s during the point-by-point and layer-by-layer forming period. It can thus realize the freeform fabrication of metallic materials and has recently been adopted in various attempts to produce BMGs [6]. To date, some Fe- [7–9], Zr- [10–12], Al- [13,14] and Ti-based [15] glass-forming alloys have been fabricated by SLM, preliminarily verifying its capabilities in producing BMGs in intricate shapes and large sizes. It is known that Cu-based BMGs usually possess a higher strength, better ductility and are relatively lower in cost [16,17]. However, the application of SLM and infrared laser in the manufacturing Cu-based BMGs is restricted by the high thermal conductivity and the high reflectivity of Cu-based alloys, resulting in greater heat loss and an inadequate melting of the powders during the SLM process.

This work seeks to uncover the structural and mechanical characteristics of SLM-fabricated Cu-based BMGs and sort out the related impact of SLM processing. The $\text{Cu}_{50}\text{Zr}_{43}\text{Al}_7$ BMG, a typical ternary Cu-based bulk glass-forming alloy, was chosen for the study and fabricated by SLM. Its structural and mechanical characteristics were analyzed.

2. Materials and Methods

$\text{Cu}_{50}\text{Zr}_{43}\text{Al}_7$ powders were prepared by argon gas atomization. The as-atomized powders with a particle size between 10 and 50 μm were selected for SLM experiments. $\text{Cu}_{50}\text{Zr}_{43}\text{Al}_7$ cylindrical and cubic samples were fabricated using a 3D printer (YLM-120 SLM, manufactured by Jiangsu Yongnian Tech. Co. Ltd., Suzhou, China). As listed in Table 1, the SLM fabrication parameters for these cylinders were as follows: the laser power $P = 150$ and 190 W; the scanning speed $v = 2000, 2200,$ and 2400 mm/s; the hatch distance $h = 0.1$ and 0.12 mm; the layer thickness $d = 0.03$ mm; and the laser energy density E was in the range of 20.8–31.7 J/mm^3 calculated using the formula $E = P / (h \times v \times d)$ (J/mm^3). The SLM fabrication process was performed under an argon atmosphere with an oxygen content of below 100 ppm. The rotation angle of the laser scanning direction of adjacent layers was 67° as shown in Figure 1a. The size of the SLM-fabricated cylinder samples was 4 mm in diameter and 8 mm in height. The samples for each experimental condition were fabricated for several repetitions at a time (as shown in Figure 1b).

Table 1. Selective laser melting (SLM) experimental parameters.

E (J/mm^3)	P (W)	v (mm/s)	h (mm)	d (mm)
31.7	190	2000	0.10	0.03
28.8	190	2200	0.10	0.03
26.4	190	2400	0.10	0.03
25.0	150	2000	0.10	0.03
24.0	190	2200	0.12	0.03
22.7	150	2200	0.10	0.03
20.8	150	2400	0.10	0.03

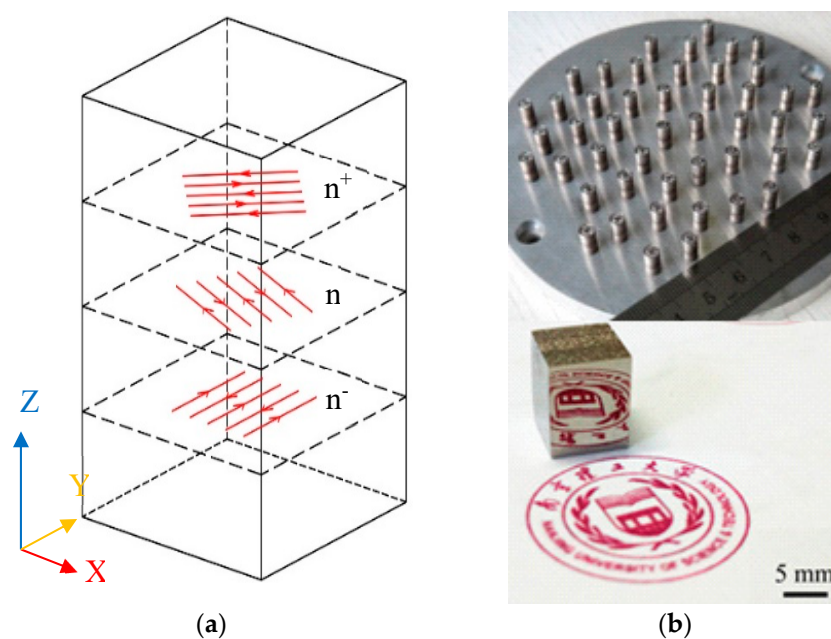


Figure 1. (a) Scanning strategy of the present selective laser melting; (b) The morphology and length of the SLM-fabricated specimens.

3. Results and Discussion

Figure 2 shows the XRD pattern of the as-atomized $\text{Cu}_{50}\text{Zr}_{43}\text{Al}_7$ powders. The pattern exhibits a characteristic broad diffraction without any detectable crystalline Bragg peaks, indicating that fully amorphous structures were obtained for the $\text{Cu}_{50}\text{Zr}_{43}\text{Al}_7$ particles with dimensions smaller than $50\ \mu\text{m}$. Obviously, the cooling rate during the gas atomization process was sufficient to suppress the formation of the crystalline phases. As shown in the inset of Figure 2, most of the as-atomized $\text{Cu}_{50}\text{Zr}_{43}\text{Al}_7$ powders exhibited spherical or near spherical shape with a smooth surface, which was conducive to the smooth running of the SLM process

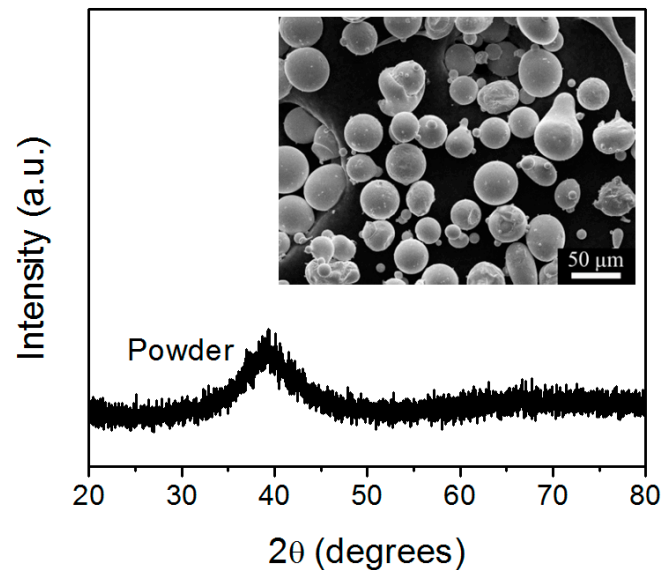


Figure 2. X-ray diffraction (XRD) pattern of the as-atomized $\text{Cu}_{50}\text{Zr}_{43}\text{Al}_7$ powders. The inset depicts a scanning electron microscopy (SEM) image of the powders.

In the present SLM process, the laser energy density was varied in order to study its influence on the amorphization of the SLM-fabricated $\text{Cu}_{50}\text{Zr}_{43}\text{Al}_7$ samples. As can be seen from Figure 1b, when the applied laser energy density was in the range of $20.8\text{--}31.7\ \text{J}/\text{mm}^3$, all the samples were successfully produced by SLM. A cubic sample with a polished lateral surface was also shown in Figure 1b. As can be seen, a mirror-like surface can be obtained by polishing, indicating the high quality of the SLM-fabricated Cu-based BMG. No obvious cracking or layer delamination was observed by visual inspection of the exterior surface. Figure 3 shows the XRD patterns taken on the cross sections of the SLM-fabricated samples under different laser energy densities. It can be seen that for the samples fabricated with the laser energy density of 31.7 , 28.8 and $26.4\ \text{J}/\text{mm}^3$, some crystalline phases occurred within the amorphous matrix, which can be attributed to crystallization at heat affect zones under relatively high laser energy. Based on previous reports [18,19], these crystalline phases can be identified as CuZr , $\text{Cu}_{10}\text{Zr}_7$ and Al_2Zr phases, respectively. Interestingly, for the samples fabricated under a low laser energy density of 20.8 , 22.7 and $24\ \text{J}/\text{mm}^3$, obvious crystalline phases could also be detected, which might have been due to the crystallization of the un-melted powders under relatively low laser energy. For the samples fabricated with a laser energy density of $25\ \text{J}/\text{mm}^3$, a nearly fully amorphous structure was obtained. However, a poor superimposed peak on the main amorphous maximum indicated that slight crystallization was inevitable in the SLM-fabricated BMG samples. In order to further investigate the crystalline phases in the SLM-fabricated Cu-based BMG sample, TEM observations were performed. Figure 4 shows the TEM images of the SLM-fabricated $\text{Cu}_{50}\text{Zr}_{43}\text{Al}_7$ BMG under a laser energy density of $25\ \text{J}/\text{mm}^3$. As can be seen from Figure 4a, many crystalline phases dispersed in the amorphous matrix. These crystalline phases were irregular in shape and their size ranged from several to dozens of nanometers. Figure 4b shows the enlarged HRTEM (high resolution

transmission electron microscopy) image of the SLM-fabricated Cu-based BMG. It is evident that the nano-sized crystalline phases precipitated from the glassy matrix. As indicated in the figure, the crystalline phases were identified as CuZr phase, consistent with the XRD result. The samples SLM-fabricated under a laser energy density of 25 J/mm^3 were used in the following studies, because of their nearly fully amorphous structure.

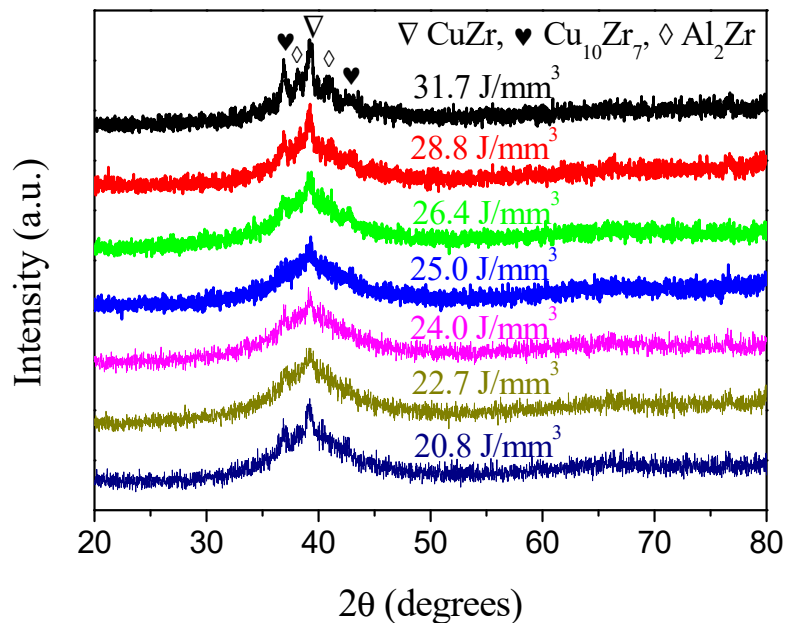


Figure 3. XRD patterns of the SLM-fabricated $\text{Cu}_{50}\text{Zr}_{43}\text{Al}_7$ specimens under different laser energy densities.

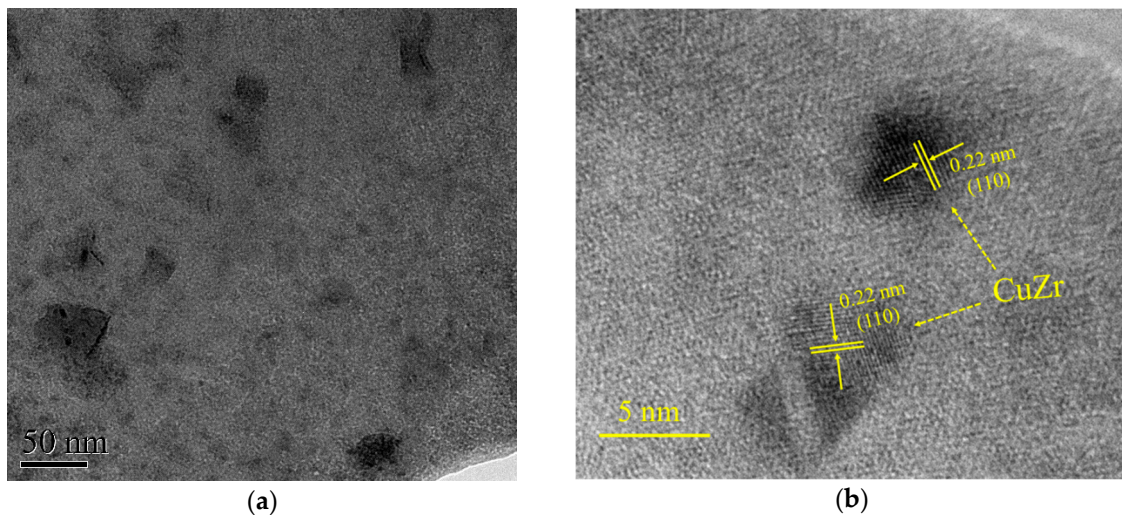


Figure 4. (a) Transmission electron microscopy (TEM) morphology and (b) high resolution transmission electron microscopy (HRTEM) image of SLM-fabricated $\text{Cu}_{50}\text{Zr}_{43}\text{Al}_7$ bulk metallic glasses (BMG) under a laser energy density of 25 J/mm^3 .

Figure 5 shows the DSC curves of as-atomized $\text{Cu}_{50}\text{Zr}_{43}\text{Al}_7$ powders and an SLM-fabricated sample with a laser energy density of 25 J/mm^3 . Both of them showed the typical features of the amorphous phase. The values of glass transition temperature (T_g) and relaxation enthalpy (ΔH_r) were 733.1 K, 1.3 J/g and 733.4 K, 1.9 J/g, respectively for the as-atomized $\text{Cu}_{50}\text{Zr}_{43}\text{Al}_7$ powders and the SLM-fabricated BMG samples. Apparently, the higher relaxation enthalpy of the SLM-fabricated BMG samples shows that they experienced structural relaxation during the SLM process. The existence of structural relaxation in the SLM-fabricated sample can be also proved by the fact that the values

of the onset temperature of crystallization (T_x , 777.7 K) for the as-atomized metallic glass powders were significantly higher than those (768.3 K) for the SLM-fabricated BMG samples. As reported previously [20], structural relaxation may lead to a decrease in the T_x of BMGs. In addition, the values of the crystallization enthalpy (ΔH_c , 49.6 J/g) for the as-atomized $\text{Cu}_{50}\text{Zr}_{43}\text{Al}_7$ powders were significantly higher than those (ΔH_c , 40.2 J/g) for the SLM-fabricated BMG sample, which indicates that partial crystallization occurred in the latter sample. SLM is a layer by layer deposition process, during which there exists a fusion zone in the current layer, a remelting zone and a heat-affected zone in the former solidified layers. The specific heat transfer status in different zones led to the occurrence of structural relaxation and partial crystallization in the SLM-fabricated BMGs. The present work implies that structural relaxation and partial crystallization co-exist in the SLM-fabricated BMGs.

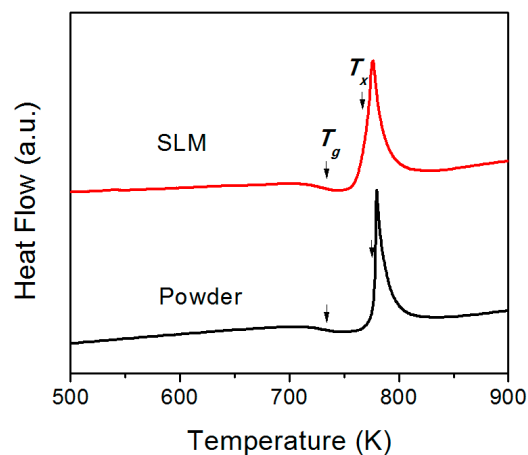


Figure 5. Differential scanning calorimetry (DSC) curves of as-atomized $\text{Cu}_{50}\text{Zr}_{43}\text{Al}_7$ metallic glass powders and the SLM-fabricated $\text{Cu}_{50}\text{Zr}_{43}\text{Al}_7$ BMG sample.

Figure 6 shows the nanoindentation load-displacement (P-h) curves measured on the cross and longitudinal sections of the SLM-fabricated $\text{Cu}_{50}\text{Zr}_{43}\text{Al}_7$ BMG cubic samples with a side length of 10 mm. Following the methods proposed by Oliver and Pharr [20], the nanoindentation hardness (H_{IT} /MPa) and elastic modulus (E_{IT}) values were calculated from the load-displacement curves. The results are listed in Table 2, together with the microscopic Vickers hardness and those from the cast Cu-based BMGs with similar compositions in the literature [22,23]. As can be seen, the hardness and elastic modulus of the SLM-fabricated $\text{Cu}_{50}\text{Zr}_{43}\text{Al}_7$ BMGs were much higher than those of the CuZrAl ternary BMGs prepared by conventional mold casting. This enhancement can mainly be attributed to structural relaxation. As reported previously [24,25], the annealing induced structural relaxation in BMGs resulting from free volume annihilation and atomic rearrangement, hindered the formation and propagation of shear bands. The hardness and elastic modulus of the relaxed BMGs were thus higher than that of the as-cast BMGs. It should be noted that the present SLM-fabricated BMG sample contained crystalline phases embedded in an amorphous matrix, as shown in Figure 3. In the previous work [26], it was revealed that the crystalline phases were softer than the amorphous matrix, thus, it is reasonable to conclude that the increased hardness in the present SLM-fabricated BMG sample was mainly due to the structural relaxation during the SLM process. Figure 7 shows the compressive engineering stress-strain curve of the SLM-fabricated $\text{Cu}_{50}\text{Zr}_{43}\text{Al}_7$ BMG rods. The compressive strength was 1044 MPa, lower than that of the as-cast Cu-based BMGs in previous reports [16,17]. The decrease in compressive strength was also found in other SLM-fabricated BMGs [15]. Obviously, the SLM-fabricated BMGs exhibited higher nanohardness and lower macro compressive strength compared to the corresponding BMGs prepared by traditional casting methods. It is worthy to reveal the reason for this phenomenon. Since SLM is a powder bed fusion additive manufacturing process, the SLM-fabricated samples are usually not completely dense and have many structural defects [7–11,15]. It is known that the macro-mechanical properties of metallic materials are strongly

affected by the presence of structural defects. The relative density of the SLM-fabricated $\text{Cu}_{50}\text{Zr}_{43}\text{Al}_7$ BMG sample under a laser energy density of 25 J/mm^3 was measured to be 0.97 by the Archimedes method. It is known that the relative density can be increased by increasing the laser energy density in the SLM process, however, in our case, a higher laser energy density than 25 J/mm^3 will lead to the obvious crystallization of the CuZrAl BMG, as shown in Figure 3.

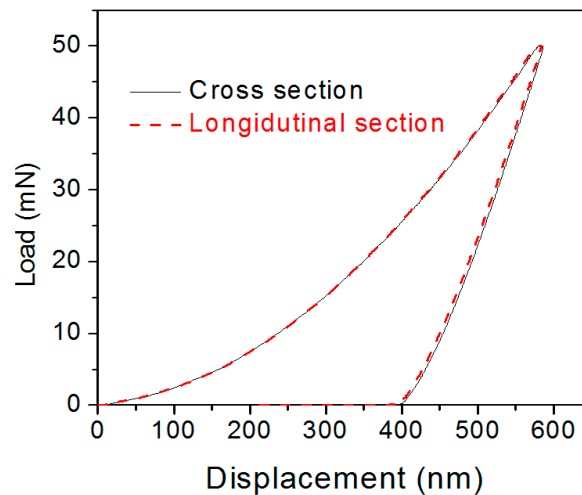


Figure 6. The fitted load-displacement (P-h) curves for nanoindentation on the cross and longitudinal sections of SLM-fabricated $\text{Cu}_{50}\text{Zr}_{43}\text{Al}_7$ BMG samples.

Table 2. The microscopic Vickers hardness ($\text{HV}_{0.5}$), nanoindentation hardness (H_{IT}), elastic modulus (E_{IT}) of SLM-fabricated $\text{Cu}_{50}\text{Zr}_{43}\text{Al}_7$ BMG, as well as some casting CuZrAl ternary BMGs.

Sample	Method	$\text{HV}_{0.5}$ (3σ)	H_{IT} (3σ , MPa)	E_{IT} (3σ , GPa)	Ref.
$\text{Cu}_{50}\text{Zr}_{43}\text{Al}_7$ (Cross section)	SLM	550.1 ± 10.9	9313.7 ± 90.6	129.1 ± 3.6	Present
$\text{Cu}_{50}\text{Zr}_{43}\text{Al}_7$ (Longitudinal section)	SLM	555.8 ± 10.6	9415.6 ± 112.5	129.6 ± 4.6	Present
$(\text{Cu}_{50}\text{Zr}_{50})_{100-x}\text{Al}_x$, $x = 0\sim 10$	as-cast	449.0~541.0	7300.0~8700.0	100.5~117.3	[20]
$\text{Cu}_{46.5}\text{Zr}_{46.5}\text{Al}_7$	as-cast	-	7430.0	118.9	[21]

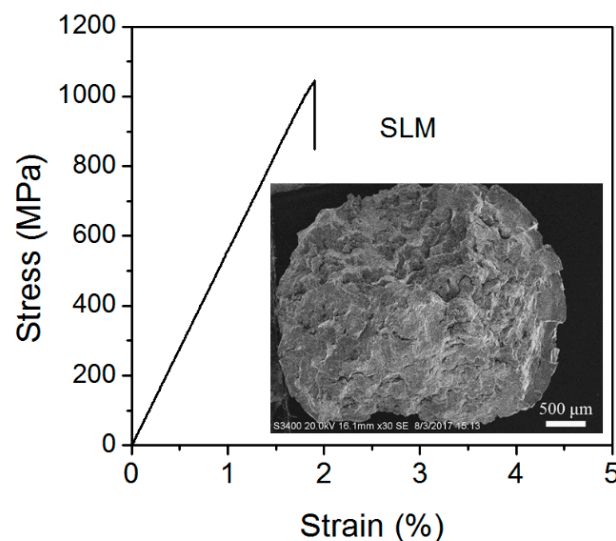


Figure 7. The stress–strain curve in the compression of SLM-fabricated $\text{Cu}_{50}\text{Zr}_{43}\text{Al}_7$ BMG rod samples. The inset depicts an SEM image of the fractured surface.

It is known that the SLM-fabricated component is formed by overlapping multi-track and multi-layer molten pools [27]. Thus, the macro-mechanical properties of SLM-fabricated component will be strongly affected by the solidified molten pools. Figure 8a,b show the morphology of the solidified molten pools in different zones on the uncorroded section parallel to the build direction of the as-fabricated $\text{Cu}_{50}\text{Zr}_{43}\text{Al}_7$ BMG. The arc-shape of the molten pool is due to the Gaussian energy distribution of the laser beam, and can be clearly seen in Figure 8a,b. In addition to the densely packed layers, a number of pores were found in the solidified molten pool boundaries of the local zones on the SLM-fabricated BMG sample, which may be the main reason for the low relative density of the SLM-fabricated $\text{Cu}_{50}\text{Zr}_{43}\text{Al}_7$ BMG. Apparently, formation of pores was much easier in the SLM-fabricated BMGs than in the SLM-produced crystalline metallic materials. This can be attributed to the highly viscous nature of the BMG melts [28–30]. Compared with the SLM-produced crystalline metallic materials, the BMGs are multicomponent alloys with large atomic size mismatches and a composition near deep eutectic. They show high viscosities that are several orders of magnitude higher than pure metal and common alloy melts [31]. The high viscosity of BMG melts causes difficulties in the spread of the melts, leading to the formation of many pores in the SLM-fabricated BMGs. The presence of pores leads to a decrease of the macro compressive strength of the SLM-fabricated BMGs.

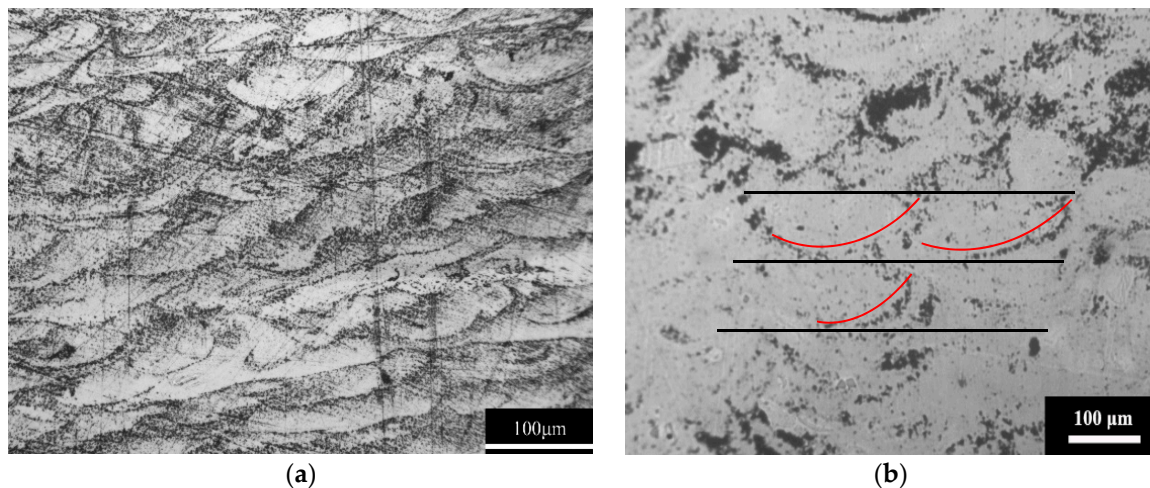


Figure 8. Morphology of solidified molten pools in different zones on the uncorroded section parallel to the build direction: (a) zones with densely packed layers; (b) zones with a number of pores.

In our work, some $\text{Cu}_{50}\text{Zr}_{43}\text{Al}_7$ BMG specimens with complex and delicate geometries were also fabricated by SLM, as shown in Figure 9, in order to evaluate the processability of the present as-atomized BMG powders. It can be seen that all the specimens have a relatively smooth surface without any macroscopic defects, which indicates that $\text{Cu}_{50}\text{Zr}_{43}\text{Al}_7$ BMG specimens can be well manufactured by the SLM method. The present work implied that SLM is a promising processing avenue for fabricating BMGs with large sizes and complex shapes that may be impossible to obtain by traditional casting methods.

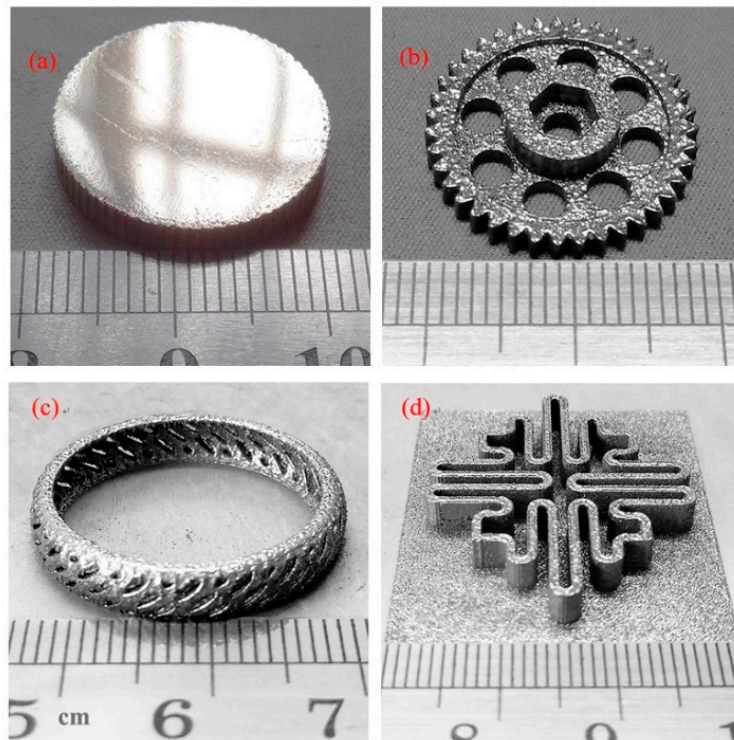


Figure 9. Some large and/or complex glassy $\text{Cu}_{50}\text{Zr}_{43}\text{Al}_7$ parts produced by SLM: (a) a disk with diameter of 20 mm; (b) a micro gear; (c) a ring with hollowed-out structure; (d) a part with labyrinth-like structure.

4. Conclusions

In conclusion, mainly amorphous $\text{Cu}_{50}\text{Zr}_{43}\text{Al}_7$ BMG specimens are fabricated by SLM. It was found that many nano-sized crystalline phases precipitated from the glassy matrix during the SLM process. The as-prepared BMG specimens without major external cracks had a number of micro-scale pores in the solidified molten pool boundaries due to the high viscosity of the BMG melts, which may be the main reason for the low relative density and high porosity of the SLM-fabricated $\text{Cu}_{50}\text{Zr}_{43}\text{Al}_7$ BMG. The hardness and elastic modulus of the SLM-fabricated $\text{Cu}_{50}\text{Zr}_{43}\text{Al}_7$ BMG was higher than those of the CuZrAl ternary BMGs prepared by conventional mold casting. This can be mainly attributed to structural relaxation during the SLM process. The presence of lots of pores resulted in a decrease in the macro compressive strength of the SLM-fabricated BMGs. Our work proved that SLM is a promising technique for the development of BMGs with complex geometries and large cross sections, and SLM processing brings significant changes to the structural and mechanical properties of BMGs.

Author Contributions: X.L., Y.D. and W.L. designed the experiments; X.L. and M.N. performed the experiments; X.L. and Y.D. analyzed the data and wrote the paper.

Funding: This work was supported by the National Natural Science Foundation of China under Project No. 51571116 and the Fundamental Research Funds for the Central Universities (No. 30915014101).

Conflicts of Interest: The authors declare no conflict of interest.

References

1. Schroers, J. Processing of Bulk Metallic Glass. *Adv. Mater.* **2010**, *22*, 1566–1597. [[CrossRef](#)] [[PubMed](#)]
2. Inoue, A.; Takeuchi, A. Recent development and application products of bulk glassy alloys. *Acta Mater.* **2011**, *59*, 2243–2267. [[CrossRef](#)]
3. Li, H.F.; Zheng, Y.F. Recent advances in bulk metallic glasses for biomedical applications. *Acta Biomater.* **2016**, *36*, 1–20. [[CrossRef](#)] [[PubMed](#)]

4. Itoi, T.; Takamizawa, T.; Kawamura, Y.; Inoue, A. Fabrication of $\text{Co}_{40}\text{Fe}_{22}\text{Nb}_8\text{B}_{30}$ bulk metallic glasses by consolidation of gas-atomized powders and their soft-magnetic properties. *Scr. Mater.* **2001**, *45*, 1131–1137. [[CrossRef](#)]
5. Choi, P.P.; Kim, J.S.; Nguyen, O.T.H.; Kwon, Y.S. $\text{Ti}_{50}\text{Cu}_{25}\text{Ni}_{20}\text{Sn}_5$ bulk metallic glass fabricated by powder consolidation. *Mater. Lett.* **2007**, *61*, 4591–4594. [[CrossRef](#)]
6. Olakanmia, E.O.; Cochran, R.F.; Dalgarno, K.W. A review on selective laser sintering/melting (SLS/SLM) of aluminium alloy powders: Processing, microstructure, and properties. *Prog. Mater. Sci.* **2015**, *74*, 401–477. [[CrossRef](#)]
7. Pauly, S.; Löber, L.; Petters, R.; Stoica, M.; Scudino, S.; Kühn, U.; Eckert, J. Processing metallic glasses by selective laser melting. *Mater. Today* **2013**, *16*, 37–41. [[CrossRef](#)]
8. Jung, H.Y.; Choi, S.J.; Prashanth, K.G.; Stoica, M.; Scudino, S.; Yi, S.; Kühn, U.; Kim, D.H.; Kim, K.B.; Eckert, J. Fabrication of Fe-based bulk metallic glass by selective laser melting: A parameter study. *Mater. Des.* **2015**, *86*, 703–708. [[CrossRef](#)]
9. Mahbooba, Z.; Thorsson, L.; Unosson, M.; Skoglund, P.; West, H.; Horn, T.; Rock, C.; Vogli, E.; Harrysson, O. Additive manufacturing of an iron-based bulk metallic glass larger than the critical casting thickness. *Appl. Mater. Today* **2018**, *11*, 264–269. [[CrossRef](#)]
10. Li, X.P.; Roberts, M.P.; O’Keeffe, S.; Sercombe, T.B. Selective laser melting of Zr-based bulk metallic glasses Processing, microstructure and mechanical properties. *Mater. Des.* **2016**, *112*, 217–226. [[CrossRef](#)]
11. Ouyang, D.; Li, N.; Xing, W.; Zhang, J.J.; Liu, L. 3D printing of crack-free high strength Zr-based bulk metallic glass composite by selective laser melting. *Intermetallics* **2017**, *90*, 128–134. [[CrossRef](#)]
12. Ouyang, D.; Li, N.; Liu, L. Structural heterogeneity in 3D printed Zr-based bulk metallic glass by selective laser melting. *J. Alloys Compd.* **2018**, *740*, 603–609. [[CrossRef](#)]
13. Li, X.P.; Kang, C.W.; Huang, H.; Zhang, L.C.; Sercombe, T.B. Selective laser melting of an $\text{Al}_{86}\text{Ni}_6\text{Y}_{4.5}\text{Co}_2\text{La}_{1.5}$ metallic glass Processing, microstructure evolution and mechanical properties. *Mater. Sci. Eng. A* **2014**, *606*, 370–379. [[CrossRef](#)]
14. Li, X.P.; Roberts, M.; Liu, Y.J.; Kang, C.W.; Huang, H.; Sercombe, T.B. Effect of substrate temperature on the interface bond between support and substrate during selective laser melting of Al–Ni–Y–Co–La metallic glass. *Mater. Des.* **2015**, *65*, 1–6. [[CrossRef](#)]
15. Deng, L.; Wang, S.H.; Wang, P.; Kühn, U.; Pauly, S. Selective laser melting of a Ti-based bulk metallic glass. *Mater. Lett.* **2018**, *212*, 346–349. [[CrossRef](#)]
16. Kim, Y.C.; Lee, J.C.; Cha, P.R.; Ahn, J.P.; Fleury, E. Enhanced glass forming ability and mechanical properties of new Cu-based bulk metallic glasses. *Mater. Sci. Eng. A* **2006**, *437*, 248–253. [[CrossRef](#)]
17. Du, Y.L.; Xu, H.W.; Chen, G.; Deng, Y. Structural and mechanical properties of a Cu-based bulk metallic glass with two oxygen levels. *Intermetallics* **2012**, *30*, 90–93. [[CrossRef](#)]
18. Zhang, Y.; Chen, J.; Chen, G.L.; Liu, X.J. Influence of yttrium addition on the glass forming ability in Cu–Zr–Al alloys. *Mater. Sci. Eng. A* **2008**, *483–484*, 235–238. [[CrossRef](#)]
19. Ning, Z.; Liang, W.; Zhang, M.; Li, Z.; Sun, H.; Liu, A.; Sun, J. High tensile plasticity and strength of a CuZr-based bulk metallic glass composite. *Mater. Des.* **2016**, *90*, 145–150. [[CrossRef](#)]
20. Zhuang, Y.X.; Wang, W.H. Effects of relaxation on glass transition and crystallization of ZrTiCuNiBe bulk metallic glass. *J. Appl. Phys.* **2000**, *87*, 8209–8211. [[CrossRef](#)]
21. Oliver, W.C.; Pharr, G.M. An improved technique for determining hardness and elastic modulus using load and displacement sensing indentation experiments. *J. Mater. Res.* **1992**, *7*, 1564–1583. [[CrossRef](#)]
22. Cheung, T.L.; Shek, C.H. Thermal and mechanical properties of Cu–Zr–Al bulk metallic glasses. *J. Alloys Compd.* **2007**, *434–435*, 71–74. [[CrossRef](#)]
23. Limbach, R.; Kosiba, K.; Pauly, S.; Kühn, U.; Wondraczek, L. Serrated flow of CuZr-based bulk metallic glasses probed by nanoindentation: Role of the activation barrier, size and distribution of shear transformation zones. *J. Non-Cryst. Solids* **2017**, *459*, 130–141. [[CrossRef](#)]
24. Ramamurty, U.; Lee, M.L.; Basu, J.; Li, Y. Embrittlement of a bulk metallic glass due to low-temperature annealing. *Scr. Mater.* **2002**, *47*, 107–111. [[CrossRef](#)]
25. Song, M.; Li, Y.Q.; Wu, Z.G.; He, Y.H. The effect of annealing on the mechanical properties of a ZrAlNiCu metallic glass. *J. Non-Cryst. Solids* **2011**, *357*, 1239–1241. [[CrossRef](#)]
26. Wu, Y.; Xiao, Y.; Chen, G.; Liu, C.T.; Lu, Z. Bulk metallic glass composites with transformation-mediated work-hardening and ductility. *Adv. Mater.* **2010**, *22*, 2770–2773. [[CrossRef](#)] [[PubMed](#)]

27. Wen, S.; Li, S.; Wei, Q.; Yan, C.; Zhang, S.; Shi, Y. Effect of molten pool boundaries on the mechanical properties of selective laser melting parts. *J. Mater. Process. Technol.* **2014**, *214*, 2660–2667.
28. Lee, K.S.; Kim, S.; Lim, K.R.; Hong, S.H.; Kim, K.B.; Na, Y.S. Crystallization, high temperature deformation behavior and solid-to-solid formability of a Ti-based bulk metallic glass within supercooled liquid region. *J. Alloys Compd.* **2016**, *663*, 270–278. [[CrossRef](#)]
29. Li, C.Y.; Zhu, F.P.; Zhang, X.Y.; Ding, J.Q.; Yin, J.F.; Wang, Z.; Zhao, Y.C.; Kou, S.Z. The rheological behavior and thermoplastic deformation of Zr-based bulk metallic glasses. *J. Non-Cryst. Solids* **2018**, *492*, 140–145. [[CrossRef](#)]
30. Hong, S.H.; Kim, J.T.; Mun, S.C.; Kim, Y.S.; Park, H.J.; Na, Y.S.; Lim, K.R.; Park, J.M.; Kim, K.B. Influence of spherical particles and interfacial stress distribution on viscous flow behavior of Ti-Cu-Ni-Zr-Sn bulk metallic glass composites. *Intermetallics* **2017**, *91*, 90–94. [[CrossRef](#)]
31. Busch, R.; Schroers, J.; Wang, W. Thermodynamics and kinetics of bulk metallic glass. *MRS Bull.* **2007**, *32*, 620–623. [[CrossRef](#)]



© 2019 by the authors. Licensee MDPI, Basel, Switzerland. This article is an open access article distributed under the terms and conditions of the Creative Commons Attribution (CC BY) license (<http://creativecommons.org/licenses/by/4.0/>).